Genes & Diseases (2022) 9, 1701–1715

Available online at www.sciencedirect.com

ScienceDirect

journal homepage: http://ees.elsevier.com/gendis/default.asp

FULL LENGTH ARTICLE

G3BP2 regulates oscillatory shear stress-induced endothelial dysfunction

Tianhan Li [a,b,1], Juhui Qiu [a,**,1], Tingting Jia [b], Yinming Liang [b], Kun Zhang [a], Wenhua Yan [a], Zhengjun Hou [a], Shiwei Yang [c], Lushan Liu [d], Wenhao Xiong [d], Yaokai Chen [e,***], Guixue Wang [a,*]

[a] *Key Laboratory for Biorheological Science and Technology of Ministry of Education, State Key Laboratory of Mechanical Transmission, State and Local Joint Engineering Laboratory for Vascular Implants, Bioengineering College of Chongqing University, Chongqing 400044, PR China*
[b] *Laboratory of Genetic Regulators in the Immune System, Henan Collaborative Innovation Center of Molecular Diagnosis and Laboratory Medicine, Xinxiang Medical University, Xinxiang, Henan 45003, PR China*
[c] *Department of Vascular Surgery, First Affiliated Hospital, Army Medical University (Third Military University), Chongqing 400038, PR China*
[d] *Institute of Cardiovascular Disease, Key Laboratory for Arteriosclerology of Hunan Province, Hunan International Scientific and Technological Cooperation Base of Arteriosclerotic Disease, Hengyang Medical College, University of South China, Hengyang, Hunan 421001, PR China*
[e] *Division of Infectious Diseases, Chongqing Public Health Medical Center, Chongqing 400030, PR China*

Received 26 May 2021; received in revised form 6 October 2021; accepted 5 November 2021
Available online 19 November 2021

KEYWORDS
Atherosclerosis;
Endothelial cells (ECs);
G3BP2;
Oscillatory shear stress (OSS);
YAP

Abstract GTPase-activating SH3 domain-binding protein 2 (G3BP2) is a mediator that responds to environmental stresses through stress granule formation and is involved in the progression of chronic diseases. However, no studies have examined the contribution of G3BP2 in the oscillatory shear stress (OSS)-induced endothelial dysfunction. Here we assessed the effects of G3BP2 in endothelial cells (ECs) function and investigated the underlying mechanism. Using shear stress apparatus and partial ligation model, we identified that stress granule-related genes in ECs could be induced by OSS with RNA-seq, and then confirmed that G3BP2 was highly and specifically expressed in athero-susceptible endothelia in the OSS regions. *G3bp2*$^{-/-}$*Apoe*$^{-/-}$ mice had significantly decreased atherosclerotic lesions associated with deficiency of G3BP2 in protecting endothelial barrier function, decreasing monocyte adhesion

* Corresponding author.
** Corresponding author.
*** Corresponding author.
E-mail addresses: jhqiu@cqu.edu.cn (J. Qiu), yaokaichen@hotmail.com (Y. Chen), guixue_wang@126.com (G. Wang).
Peer review under responsibility of Chongqing Medical University.
[1] These authors contributed equally to this work.

https://doi.org/10.1016/j.gendis.2021.11.003

to ECs and inhibiting the proinflammatory cytokine levels. Furthermore, loss of G3BP2 diminished OSS-induced inflammation in ECs by increasing YAP nucleocytoplasmic shuttling and phosphorylation. These data demonstrate that G3BP2 is a critical OSS regulated gene in regulating ECs function and that G3BP2 inhibition in ECs is a promising atheroprotective therapeutic strategy.

Introduction

Cardiovascular disease is a multifactorial vascular disease and remains the leading cause of mortality and morbidity worldwide.[1,2] Since many forms of cellular stress, including oxidative stress, immune stress, endoplasmic reticulum stress and oscillatory shear stress (OSS), can result in atherogenesis,[3–5] atherosclerosis is considered to be a chronic disease in response to a dysfunctional stress response. Various cellular stresses, such as heat shock, oxidative stress, viral infection and mechanical force,[6] can induce the formation of stress granules (SGs), a kind of liquid–liquid phase separation.[7] Transient SGs assembly is a cytoprotective response to adverse environmental conditions, whereas continuous SG assembly will lead to chronic diseases, such as Alzheimer's disease, cancer progression and metastasis.[7–10]

Because of long-term exposure to OSS of blood flow, atherosclerosis develops preferentially near arterial bifurcations, branching ostia and curvature.[11] Endothelial cells (ECs), localized inside vessels, are exquisitely sensitive to the haemodynamic force generated by blood flow, and endothelial dysfunction caused by OSS plays a vital role in atherosclerotic development and progression.[12,13] Recently, a study indicated that SGs are induced during atherogenesis and increased with vascular disease progression.[14] They mainly focus on SGs in smooth muscle cells (SMCs) and macrophages, but the role and mechanism of SGs in ECs due to OSS exposure are unclear.

G3BP2 is a major component of SGs and plays a vital role in regulating SGs formation induced by cellular stress by controlling mRNA stability and translation[15,16] and is highly associated with phase separation in dysfunctional. Recent studies have suggested that OSS-induced vascular inflammatory diseases are associated with mRNA stability and translation in response to environmental stresses.[17–19] And endothelial integrin-YAP signal pathway was activated under OSS, which led to endothelial inflammation and atherogenesis.[20] We hypothesized that OSS-induced atherogenesis may be related to G3BP2-associated SG formation in ECs and G3BP2 may involve in integrin-YAP mediated atherogenesis.

To the best of our knowledge, this study is the first to show OSS upregulated G3BP2 expression and SGs formation with endothelial dysfunction. Using RNA sequencing, immunofluorescence, immunohistochemistry, quantitative PCR, and Western blotting analysis as well as surgical intervention, a flow chamber system and *G3bp2*$^{-/-}$*Apoe*$^{-/-}$ mice, we confirmed that loss of G3BP2 could inhibit OSS-induced atherosclerotic lesions formation in *Apoe*$^{-/-}$ mice by enhancing endothelial barrier function and decreasing proinflammatory cytokine levels. Moreover, endothelial G3BP2 was found to regulate the phosphorylation of YAP, a flow-response transcriptional coregulator induced by OSS.[21] Together, our results identify that G3BP2 represents a critical controller of OSS-induced endothelial dysfunction, and the inhibition of G3BP2 in ECs reduces atherosclerosis formation.

Materials and methods

Mice

Six to 8-week-old *Apoe*$^{-/-}$ mice were purchased from Beijing Vital River Laboratory Animal Technology Co., Ltd., and *G3bp2* knockout mice (*B6/JGpt-G3bp2em2Cd1082/Gpt*) were generated by the Model Animal Research Center of Nanjing University. Eight-week-old *Apoe*$^{-/-}$, *G3bp2*$^{+/-}$*Apoe*$^{-/-}$ or *G3bp2*$^{-/-}$*Apoe*$^{-/-}$ mice were obtained by *G3bp2*$^{+/-}$*Apoe*$^{-/-}$self-crossing (Fig. S1) and used for all animal studies according to the approved protocol of the Committee on Animal Care at Xinxiang Medical University, and all procedures were conformed to the guidelines from Directive 2010/63/EU of the European Parliament on the protection of animals used for scientific purposes. Mice were identified with PCR.

Partial ligation model

Apoe$^{-/-}$, *G3bp2*$^{+/-}$*Apoe*$^{-/-}$ or *G3bp2*$^{-/-}$*Apoe*$^{-/-}$ mice (7–8 weeks) were anaesthetized by continuous inhaling in 1.5%–2% isoflurane (Abbott Laboratories, China) during surgery (15–20 min) and carotid arteries were separated using operating instruments. The right carotid artery (RCA) was separated but not ligated as sham group, and the left carotid artery (LCA) was separated and ligated as ligation group. For ligation, we ligated three branches of the LCA, including the external carotid artery (ECA), internal carotid artery (ICA) and occipital artery (OA) using a 9–0 ligature, but the superior thyroid artery (STA) was not ligated. Ultrasonography was used to measure the velocity of blood flow 24 h after ligation via the Vevo 2100 animal ultrasound instrument (VisualSonics, Canada). All mice were fed a high-fat diet (MD12015, Jiangsu Medicience Biomedical Co., Ltd, the concentration of cholesterol was 0.15%) for 4 weeks after surgery. Mice were sacrificed by exsanguination in isoflurane and carotids were collected.

Cell culture, shear stress apparatus and lentiviral infections

The plasma fibronectin (ScienCell, Cat# 8248)-coated culture vessels (40 μg/ml) were prepared 12 h before subculture. Primary human umbilical vein endothelial cells (HUVECs) (ScienCell, Cat# 8000) were maintained in endothelial cell medium (ECM, ScienCell, Cat# 1001) containing 5% foetal bovine serum (FBS, ScienCell, Cat# 0025), 1% penicillin/streptomycin (ScienCell, Cat# 0503) and endothelial growth supplement (EGS, ScienCell, Cat# 1052) at 37 °C in an incubator containing 5% CO_2, and up to eight passages were used.

HUVECs were seeded on fibronectin-coated slides. After culture for 12 h in ECM, the slides were treated with shear stress using a parallel-plate flow chamber with a piston pump that exerts a frequency of 1 Hz and 0.5 ± 4 dyn/cm^2 of shear stress according to our previous study.[12] Briefly, the fluid shear stress (τ) was calculated as this equations: $\tau = 6Q\mu/wh^2$, where Q was the flow volume and μ was the viscosity of the ECM. The flow chamber was created by a gasket with dimensions of 5 cm in length, 2.5 cm in width (w) and 0.025 cm in height (h). Samples were collected at 6 h after exerting shear stress.

The U6/RFP-Puro lentiviral vectors for G3BP2 were purchased from GenePharma and transfected into second or third generation primary HUVECs in opti-MEM (Gibco, Cat#31985062) supplemented with 5 μg/mL polybrene. After transfection for 12 h, the medium was changed to ECM (containing 2 μg/mL puromycin). The efficiency of transfection was checked using a fluorescence microscope (Olympus, Japan).

RNA sequencing and analysis

Total RNA samples for Next-Generation Sequencing (NGS) were extracted from HUVECs treated with or without OSS for 6 h, and OSS-treated sh-Control and sh-G3BP2 HUVECs using TRIzol (Takara Biomedical Technology, 9109). Quality assurance for the RNA samples were carried out using Nanodrop 2100 (Thermo, US), Qubit 3.0 (Thermo, US) and Agilent 2100 Bioanalyzer (Agilent Technologies, US). RNA libraries were generated using the Illumina Truseq Stranded Total RNA kit. Then, their concentrations and insert sizes were performed using Qubit 3.0 and Agilent 2100 Bioanalyzer, respectively. Paired-end sequencing was performed on an Illumina Hiseq 2500 sequencing platform. Raw read were filtered using the HISAT2 package (http://ccb.jhu.edu/software/hisat2/index.shtml), and then mapped to the reference human genome GRCh 38. The differentially expressed genes (Fold change >2 or < -2, false discovery rate <0.05) were performed on enrichment analysis (GSEA), classification by gene ontology categories and DAVID tool. And pathway enrichment was performed on the Kyoto Encyclopedia of Gene and Genomes (KEGG) Database. Gene expression data have been uploaded to NCBI for public availability under accession PRJNA706049.

Immunofluorescence

The frozen sections of carotid arteries were incubated at 60 °C for 2 min, and the carotid arteries or aortic arches were fixed with 4% paraformaldehyde for 30 min. Then the samples were washed with PBS and permeabilized/blocked with 0.1% Triton-X100 (in 5% BSA). Subsequently, the samples were added with the primary antibody in a wet box at 4 °C overnight. Primary antibodies included anti-G3BP2 (ab86135), anti-CD31 (AF3628), anti-YAP (Cell Signaling Technology, #14074), anti-pYAP (Cell Signaling Technology, #13008), anti-VE-cadherin (sc-9989) and anti-integrin β3 (sc-365679). After the samples were washed with PBST (PBS with 0.1% Tween-20) 5 times, the samples were incubated with secondary antibodies for 1 h and then with DAPI for 10 min at room temperature (protected from light). The fluorescent signal of sections was detected by SP8 confocal microscopy (Lecia, Germany).

Permeability experiment

The *in vivo* endothelial barrier function was measured by using Evans blue. Eight-week-old mice were injected with 5 mg/kg 1% Evans blue (#E2129, Sigma) via the tail vein for 45 min. Then, they were anaesthetized and perfused with normal saline. Evans blue dye in the descending aorta was photographed via a digital camera (Nikon, Japan), extracted by formamide and quantified using spectrophotometry (Thermo, US).

Immunohistochemical and morphometric analyses

The paraffin-embedded sections of carotid arteries were dewaxed in xylene two times for 10 min, rehydrated in descending grades of ethanol (each grade for 5 min), and treated with sodium citrate-induced antigen retrieval for 10 min at 95 °C. Then the endogenous enzyme activity was inactivated in 3% H_2O_2 for 10 min at room temperature. Sections were blocked with QuickBlock Reagent (Beyotime Biotechnology, P0260) for 10 min and incubated with the following primary antibodies, respectively: anti-ICAM (10020-1-AP), VCAM (66294-1-lg), anti-CD31 (AF3628), anti-MCP-1 (25542-1-AP). After the sections were washed in PBS 5 times, the sections were incubated with secondary antibodies for 30 min and stained with DAB at room temperature. Subsequently, the sections were counterstained with haematoxylin, dehydrated in descending grades of ethanol, and fixed with neutral balsam. Images were acquired using a NIKON Eclipse Ci microscope with NIS Ver46000 software and analyzed using Image J software.

Quantitative PCR

RNA was extracted from different treated HUVECs using RNAiso Plus (#9109, Takara Biomedical Technology) following the manufacturer's instructions and detected by using a Nanodrop 2000 spectrophotometer (Thermo, US). Quantitative PCR for specific genes was performed using the reverse transcription PCR Reagent Kit (Takara Biomedical Technology Co., Ltd., RR047A) and measured by a Roche Lightcycler 480 Detection System. Gene primers used for quantitative PCR are shown in Table S1.

Western blotting

Total protein was extracted from HUVECs or tissues using cold lysis buffer (P0013, Beyotime Biotechnology) and determined using a BCA Protein Assay Kit (P0010, Beyotime Biotechnology) and microplate reader (BioTek, US). Approximately 30 μg of total protein was loaded on an SDS-polyacrylamide gel. After transmembrane transfer, the membranes were blocked with 5% BSA for 1 h and incubated with specific primary antibodies, respectively: anti-G3BP2 (ab86135), anti-GAPDH (Cell

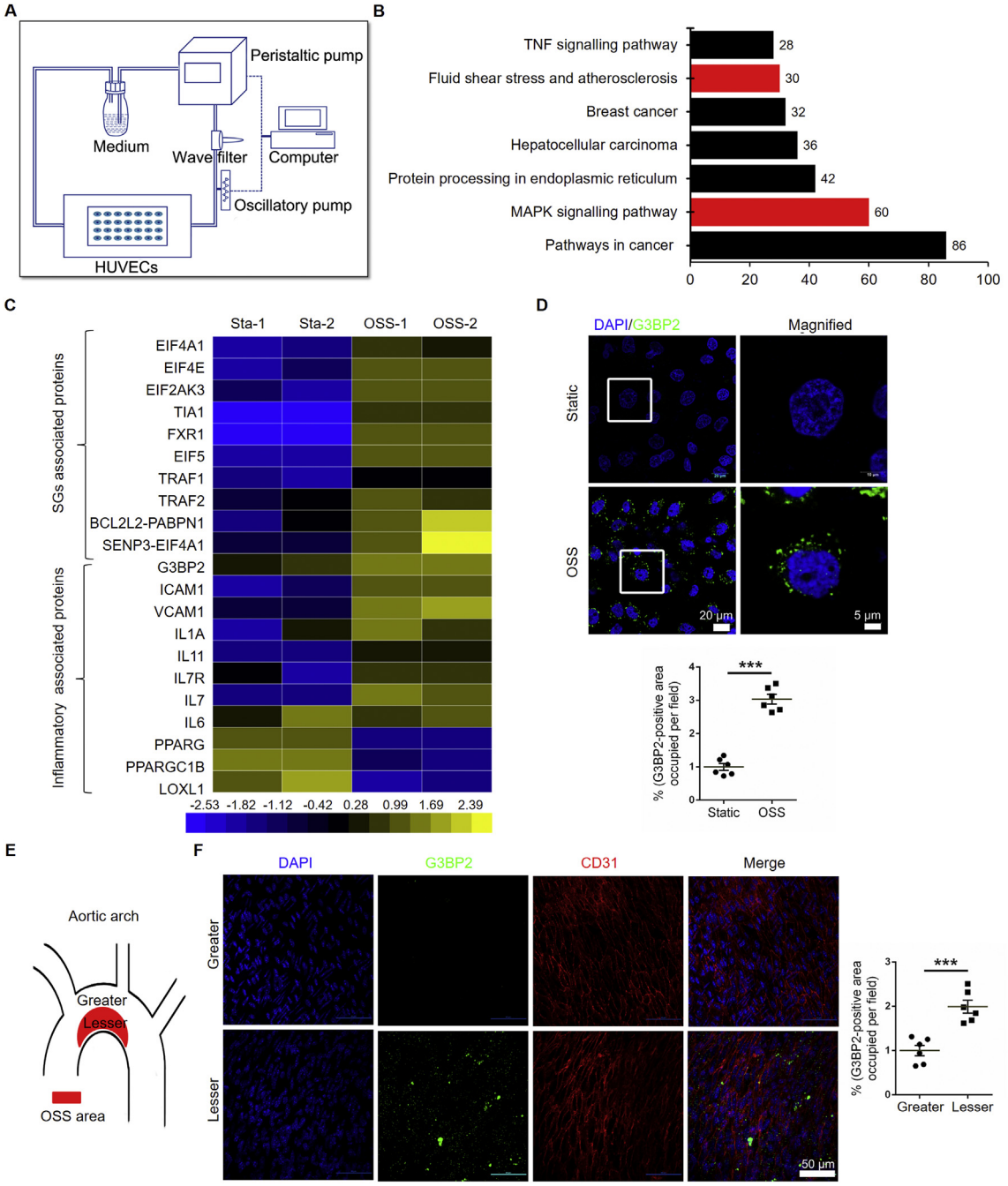

Figure 1 OSS increases the expression of G3BP2 in ECs. **(A)** Diagram of a mechanical loading device with a parallel flow chamber. **(B)** KEGG enrichment pathway analysis of the mRNA profile in HUVECs treated with OSS. Red bar means the pathway we interested in. **(C)** Heatmap of selected significant mRNAs in SGs and inflammation. **(D)** Representative images showing immunofluorescence staining of G3BP2 (green) markers in HUVECs treated with static or OSS for 6 h and statistical data of G3BP2 in HUVECs ($n = 6$). Scale bars, 20 μm in the original image and 5 μm in the magnified image. **(E)** Diagram of aortic arch (red shading indicates the lesser area of aortic arch) **(F)** Representative photomicrographs showing *en face* staining of G3BP2 (green) and CD31 (red) in the aortic arch of *Apoe*$^{-/-}$ mice fed a normal diet for 8 weeks, and quantitative analysis of the G3BP2-positive area in ECs ($n = 6$). Scale bars, 50 μm. All data shown are mean ± SEM and are analyzed using the unpaired two-tailed Student's *t*-test, ***$P < 0.001$.

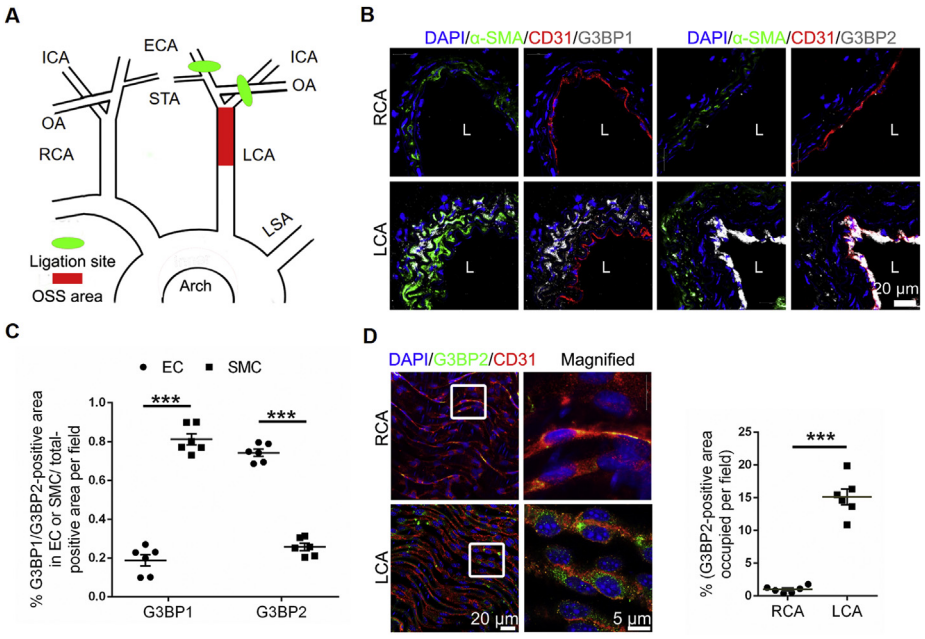

Figure 2 G3BP2, not G3BP1, is sensitive to shear stress. **(A)** Diagram of the partial ligation model (green shading indicates the ligation site, and red shading indicates the OSS area). **(B)** Representative images showing immunofluorescence staining of nucleus (blue), α-SMA (green), CD31 (red), G3BP1 or G3BP2 (white) in the LCA of partial ligation *Apoe*$^{-/-}$ mice on a high-fat diet for 4 weeks. L means lumen. Scale bars, 20 μm. **(C)** Quantitative analysis of G3BP1 and G3BP2 levels in ECs and SMCs ($n = 6$). Scale bars, 20 μm in the original image and 5 μm in the magnified image. **(D)** Representative photomicrographs showing *en face* staining of G3BP2 (green) and CD31 (red) in the carotids of *Apoe*$^{-/-}$ mice after ligation for 24 h and quantitative analysis of G3BP2 levels in ECs ($n = 6$). Scale bars, 20 μm in the original image and 5 μm in the magnified image. All data shown are mean ± SEM and are analyzed using the unpaired two-tailed Student's *t*-test. ***$P < 0.001$; *ns*, not significant.

Signaling Technology, #5174), anti-YAP (Cell Signaling Technology, #14074), anti-pYAP (Cell Signaling Technology, #13008). After the membranes were washed in TBS 5 times, the membranes were incubated with horseradish peroxidase-conjugated secondary antibodies and detected by the ECL Plus Kit (P0018S, Beyotime Biotechnology).

Monocyte adhesion assay

Monocyte adhesion induced by dysfunctional ECs was carried out using a shear stress apparatus, as previously described.[12] Briefly, HUVECs were subjected to either static or OSS for 6 h and then activated by 40 μg/mL ox-LDL in serum-free ECM for 6 h at 37 °C. Separately, THP-1 cells cultured in RPMI medium (Solarbio, Cat#31800) were labelled with BCECF-AM (2 μM, medium dilution). After the cells were washed with DPBS (ScienCell, Cat#0303), HUVECs were exposed to labelled THP-1 cells for 30 min. The non-adherent THP-1 cells were washed away with DPBS. The adherent THP-1 cells were imaged under a fluorescence microscope and counted using Image J software.

Inhibition treatment

Sh-Control and sh-G3BP2 HUVECs were treated with OSS and PBS/inhibitor for 6 h 10 mM verteporfin (HY-B0146, MedChemExpress) was carried out to inhibit the YAP nucleus translocation and 40 μM integrin β3 blocking peptide (sc-365679P, Santa Cruz Biotechnology) was used to inhibit the integrin β3.

Statistical analysis

Statistical analyses were performed using GraphPad Prism 6.0. The results are reported as the mean ± SEM. Statistical significance between 2 groups was evaluated with Student's *t* test (unpaired, two-tailed) and statistical significance among multiple groups was analyzed using ANOVA followed by Bonferroni's multiple comparison test. A significant difference was accepted at the level of probability less than 0.05. All biochemical experiments and representative images were performed in at least three independent experiments.

Results

G3BP2 and SG-related genes in ECs could be induced by OSS *in vitro*

The formation of SG plays an indispensable role in the stress response. Because ECs are sensors of shear stress, we investigated the underlying genes that participated in OSS-induced EC dysfunction through a parallel flow chamber device,[22] via next-generation sequencing (Fig. 1A). KEGG enrichment analysis revealed seven enriched pathways, including 'MAPK signaling pathway' and 'fluid shear stress and atherosclerosis' (Fig. 1B, Fig. S2), from 2399 differentially expressed genes, which including 902 downregulated and 1497 upregulated (Fig. S3). Heat map analysis of the

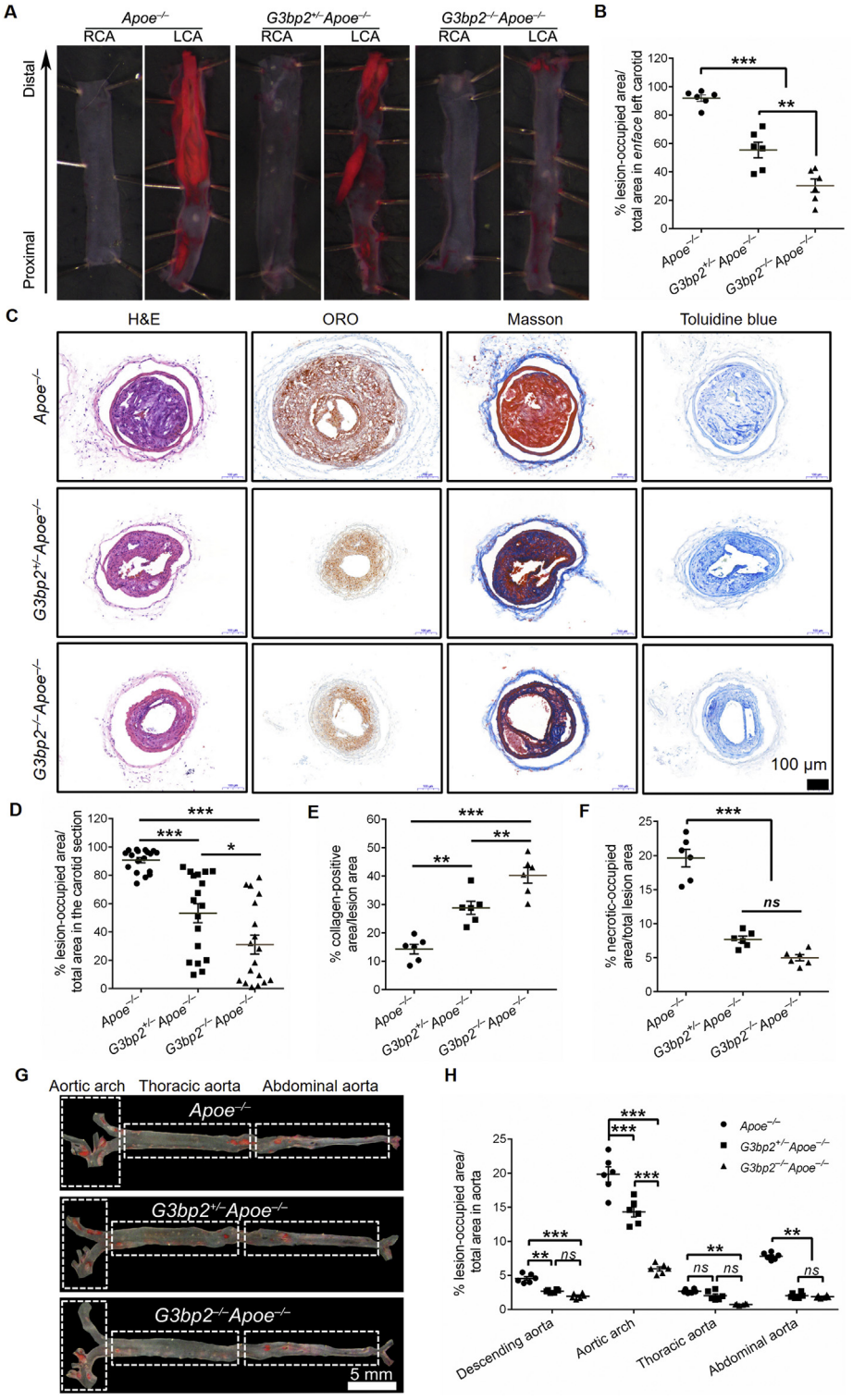

Figure 3 Loss of G3bp2 reduces OSS-induced atherosclerotic lesion formation. **(A)** Plaque area in carotid artery in partial ligation *Apoe*$^{-/-}$, *G3bp2*$^{+/-}$*Apoe*$^{-/-}$ and *G3bp2*$^{-/-}$*Apoe*$^{-/-}$ mice on a high-fat diet for 4 weeks were analyzed by *en face* ORO staining. **(B)** Percentage of lesion occupied area *vs.* total area of *enface* carotid from mice ($n = 6$). **(C)** Sections of the LCA were stained with H&E, ORO, Masson and toluidine blue staining. Scale bar, 100 μm. **(D)** Percentage of luminal surface occupied by lesion in carotid ($n = 18$ sections from 6 mice, 3 sections per mouse, including distal, middle and proximal carotid section). **(E, F)** Quantification of collagen area or necrotic area in lesion area in individual mice ($n = 6$). **(G)** Representative ORO stained descending aortas from *Apoe*$^{-/-}$, *G3bp2*$^{+/-}$*Apoe*$^{-/-}$ and *G3bp2*$^{-/-}$*Apoe*$^{-/-}$ mice fed a normal diet for 35 weeks. Scale bar, 5 mm. **(H)** Quantitative analysis of the descending aorta, aortic arch, thoracic aorta and abdominal aorta is shown ($n = 6$). All values are mean ± SEM and are analyzed by one-way ANOVA followed by Bonferroni's multiple comparison test. *$P < 0.05$; **$P < 0.01$; ***$P < 0.001$; *ns*, not significant.

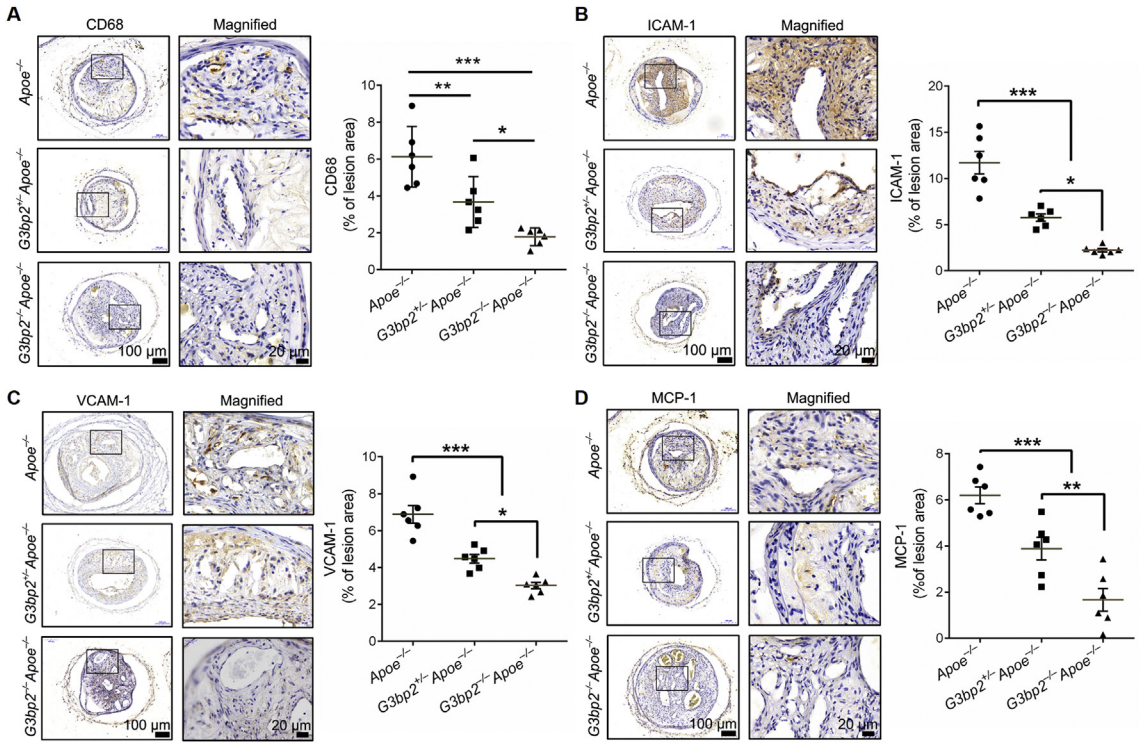

Figure 4 Loss of G3BP2 decreases the levels of proinflammatory cytokines in the lesion area. Representative photomicrographs showing immunohistochemical staining of CD68 **(A)**, ICAM-1 **(B)**, VCAM-1 **(C)** and MCP-1 **(D)** in the carotid sections of different experimental groups, and quantitative analysis of positively stained lesion areas *vs*. total lesion area for ICAM-1, VCAM-1, CD68 and MCP-1 ($n = 6$). Scale bars, 100 μm in the original image and 20 μm in the magnified image. All data shown are mean ± SEM and are analyzed by one-way ANOVA followed by Bonferroni's multiple comparison test. *$P < 0.05$, **$P < 0.01$, ***$P < 0.001$.

mRNA profile showed that OSS-induced EC inflammation-related genes, such as intercellular adhesion factor 1 (ICAM-1) and vascular cell adhesion molecule 1 (VCAM-1) were highly expressed, which is consistent with previous reports.[23,24] The expression of G3BP2 was significantly increased in HUVECs treated with OSS, together with other components of SGs (Fig. 1C, S4). The results were confirmed by immunofluorescence, and G3BP2 was highly expressed in OSS-treated ECs *in vitro* (Fig. 1D). Furthermore, we detected the expression of G3BP2 in the aortic arch of *Apoe*$^{-/-}$ mice fed a normal diet or high-fat diet for 8 weeks. These results demonstrated that the expression level of G3BP2 at the lesser curvature of the aortic arch was much higher than that at the greater curvature in *Apoe*$^{-/-}$ mouse aortic ECs (Fig. 1E, F).

G3BP2, but not G3BP1, in ECs is sensitive to OSS *in vivo*

To investigate the expression of G3BPs *in vivo*, we established the partial ligation model (Fig. 2A) using *Apoe*$^{-/-}$ mice.[12] The results of ultrasonography showed that the obvious OSS in the LCA was produced compared with the unidirectional shear stress in the RCA after ligation for 24 h (Fig. S5), which was consistent with previous study.[25] We detected both G3BP1 and G3BP2 in the LCA of ligated *Apoe*$^{-/-}$ mice fed a high-fat diet for 4 weeks, and the results showed that G3BP1 was mainly expressed in SMCs and that G3BP2 was mainly expressed in ECs (Fig. 2B). The expression of G3BP1 in the ECs had no significant change, while the expression of G3BP2 in the ECs of the LCA was highly increased compared with that in the ECs of the RCA in *Apoe*$^{-/-}$ mice after ligation for 24 h (Fig. 2C, D). Together, these results suggested that G3BP2, not G3BP1, was highly and specifically expressed in the ECs of the OSS area *in vivo*.

Depletion of G3BP2 inhibits the focal distribution of atherosclerotic lesions induced by OSS

To further investigate the function of G3BP2 in OSS induced atherosclerosis formation, *G3bp2* and *Apoe* double-knockout mice were generated by crossing of *G3bp2*$^{+/-}$*Apoe*$^{-/-}$ mice, which were obtained from fourth generation backcrossing between *G3bp2*$^{+/-}$ mice and *Apoe*$^{-/-}$ mice. Since monocytes play an important role in the formation of atherosclerosis, we detected the monocyte percentages in the blood and spleens of mice with different phenotypes and the results showed no significant difference among them (Fig. S6).

Then, carotid artery ligation models were established by using three different mouse genotypes, including *G3bp2*$^{-/-}$*Apoe*$^{-/-}$, *G3bp2*$^{+/-}$*Apoe*$^{-/-}$, and *Apoe*$^{-/-}$, and these mice were fed a 4-week high-fat diet after ligation according to a previous study.[25] *Enface* oil red O (ORO) staining of the LCA showed that the atherosclerotic plaque

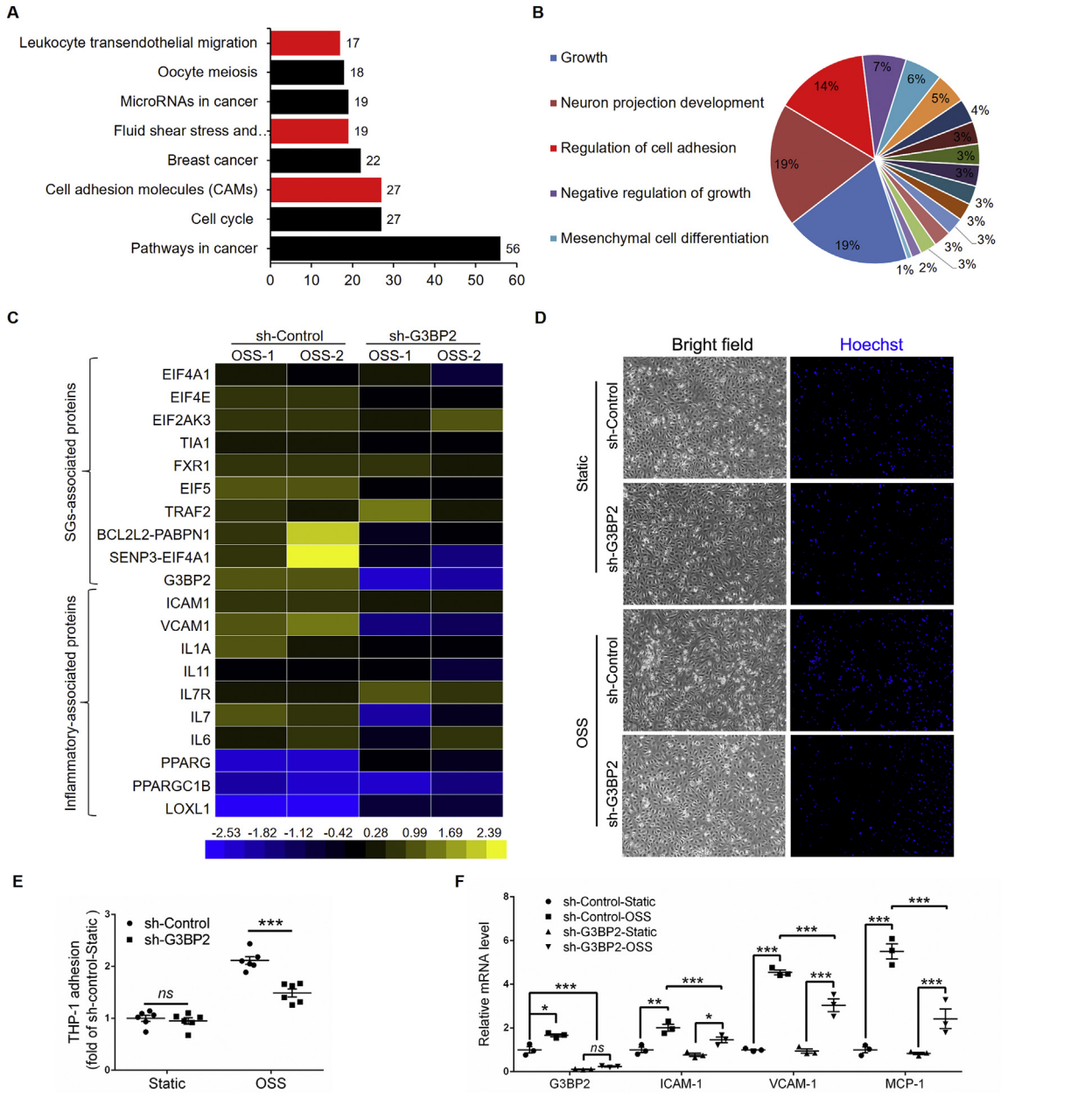

Figure 5 Knockdown of G3BP2 reduces OSS-induced monocyte adhesion. **(A)** KEGG enrichment pathway analysis and GO enrichment analysis **(B)** for the mRNA profile in HUVECs transfected with G3BP2. Red bar means the pathway we interested in. **(C)** Heatmap of selected significant mRNAs in SGs and inflammation. **(D)** THP-1 monocyte adhesion and quantification **(E)** in sh-Control and sh-G3BP2 cells under static or OSS ($n = 6$). THP-1 cells were stained with Hoechst. Image magnification at 40 $\times$. Values are mean $\pm$ SEM and are analyzed using the unpaired two-tailed Student's *t*-test. ***$P < 0.001$; *ns*, not significant. **(F)** Relative mRNA levels of G3BP2, ICAM-1, VCAM-1 and MCP-1 in sh-Control and sh-G3BP2 HUVECs treated with static or OSS ($n = 6$). Values are mean $\pm$ SEM and are analyzed by one-way ANOVA followed by Bonferroni's multiple comparison test. *$P < 0.05$; **$P < 0.01$; ***$P < 0.001$.

in both heterozygous and homozygous mice ($G3bp2^{+/-}Apoe^{-/-}$, 55.39%; $G3bp2^{-/-}Apoe^{-/-}$, 30.33%) was reduced compared with that in the control ($Apoe^{-/-}$, 91.89%) (Fig. 3A, B). Morphological examination in carotid sections revealed features of atherosclerotic lesions with plenty of lipid deposits and areas predominantly composed of fibrous tissue. As shown in Figure 3C, D, the percentage of total area occupied by lesion area was significantly smaller in $G3bp2^{+/-}Apoe^{-/-}$ (53.25%) and $G3bp2^{-/-}Apoe^{-/-}$ (31.06%) mice than in $Apoe^{-/-}$ (90.64%) mice. Masson staining showed that the collagen area percentage in $G3bp2^{+/-}Apoe^{-/-}$ (28.82%) and $G3BP2^{-/-}Apoe^{-/-}$ (40.26%) mice was increased compared with that in $Apoe^{-/-}$ mice (14.32%) (Fig. 3E). Toluidine blue staining showed that the necrotic area percentage in $G3bp2^{+/-}Apoe^{-/-}$ (7.70%) and $G3bp2^{-/-}$ $Apoe^{-/-}$ (4.99%) was significantly decreased compared with that in the control $Apoe^{-/-}$ mice (19.62%) (Fig. 3F).

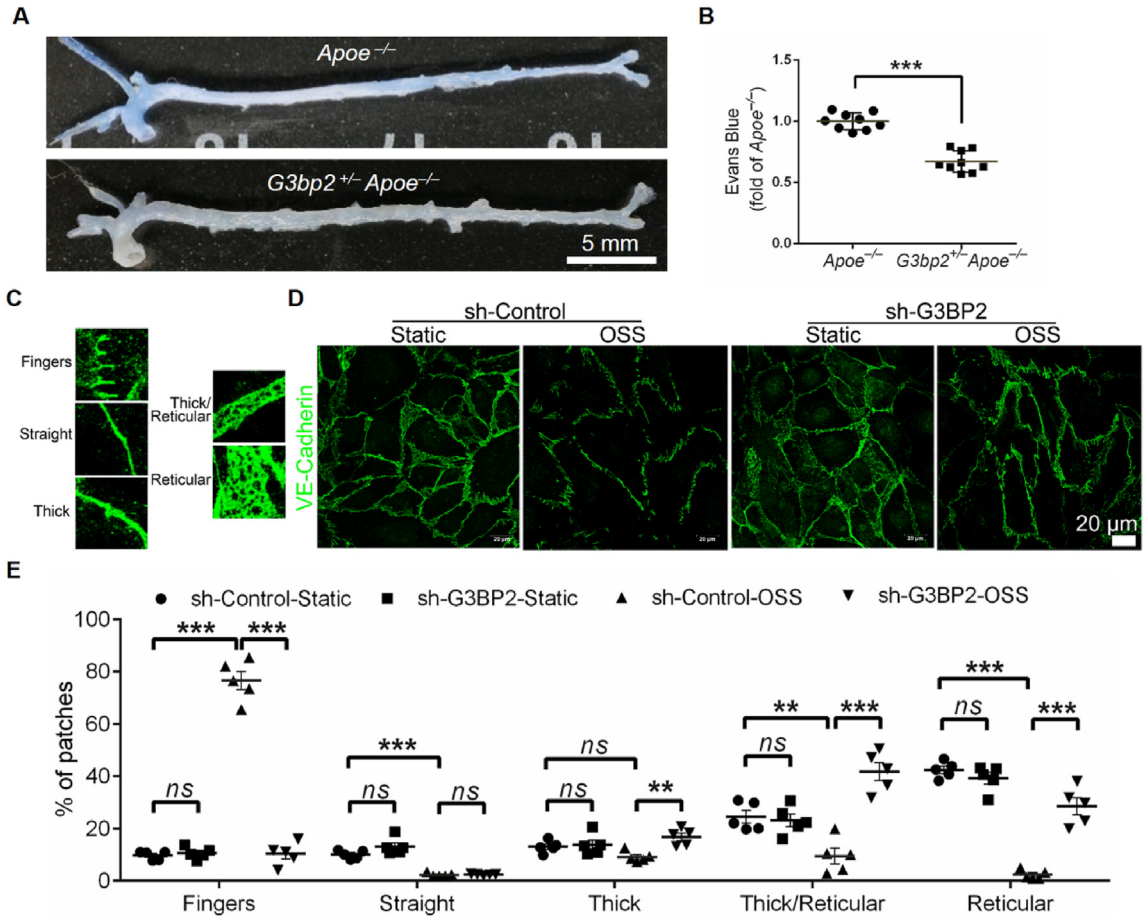

Figure 6 Deficiency of G3BP2 reduces leakage of EC layer. **(A)** Representative images showing Evans blue dye in descending aortas of *Apoe*$^{-/-}$ and *G3bp2*$^{+/-}$*Apoe*$^{-/-}$ mice. **(B)** Quantification of the OD 620 nm of Evans blue in the aortas ($n = 9$). Values are mean ± SEM and are analyzed using the unpaired two-tailed Student's *t*-test. ***$P < 0.001$. **(C)** Morphological analysis of VE-Cadherin used for manual classification in five categories: fingers, straight, thick, thick/reticular and reticular adherence junctions. **(D)** Representative images showing immunofluorescence of VE-Cadherin in HUVECs treated with OSS. **(E)** Morphological assessment of VE-Cadherin in HUVECs ($n = 5$). Values are mean ± SEM and are analyzed by one-way ANOVA followed by Bonferroni's multiple comparison test. Scale bar, 20 μm **$P < 0.01$; ***$P < 0.001$.

Apoe$^{-/-}$ mice suffer serious atherosclerosis if they fed a short-term high-fat diet or a long-term normal diet, and the atherosclerotic lesions in *Apoe*$^{-/-}$ mice are related to OSS.[26] As shown in Figure 3G and H, the percentages of lesion-occupied area in the atheroprone area in *G3bp2*$^{+/-}$*Apoe*$^{-/-}$ and *G3bp2*$^{-/-}$*Apoe*$^{-/-}$ mice were significantly reduced compared with that in *Apoe*$^{-/-}$ mice fed a normal diet for 35 weeks. Combined, these data indicated that loss of G3BP2 could reduce OSS-induced plaque formation.

Depletion of G3BP2 inhibits atherogenesis induced by OSS by lowering the level of inflammatory cytokines

Among the multiple factors that could induce atherosclerosis in *Apoe*$^{-/-}$ mice, lipid-related factors are the most important causes.[27] Interestingly, the results showed that there were similar body weight and lipid levels, including total cholesterol (TC), triglyceride (TG), high-density lipoprotein (HDL) and low-density lipoprotein (LDL), among the three groups (Fig. S7), which suggested that the atherogenesis effect of G3BP2 was unlikely to be associated with lipid metabolism. Given that the expression of inflammatory genes in response to atheroprone shear stress *in vivo* was the critical step for atherosclerosis, proinflammatory cytokines and CD68, the marker of macrophages, were determined by immunohistochemical analysis. The results revealed that the expression of VCAM-1, ICAM-1 and MCP-1, and macrophages in the lesion area were significantly decreased (Fig. 4).

Taken together, these data demonstrated that G3BP2 was a critical mediator of the ECs response to OSS, and the depletion of G3BP2 could inhibit atherosclerotic plaque formation and decrease the levels of proinflammatory cytokines and macrophages in plaques induced by OSS.

Knockdown of G3BP2 could enhance the barrier of the EC layer

To further investigate the underlying mechanism of G3BP2 in OSS induced endothelial function, we analyzed mRNA

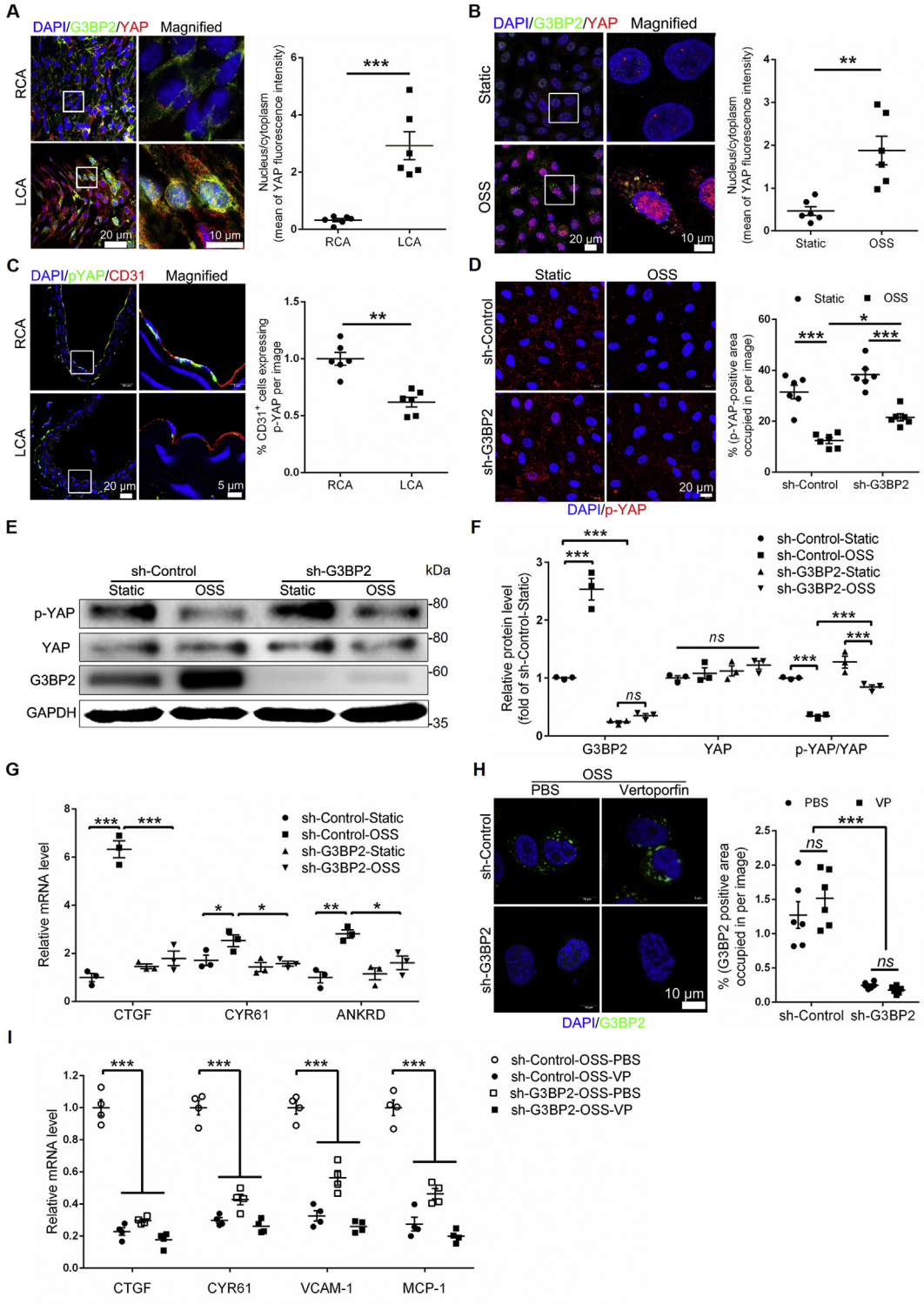

Figure 7 G3BP2 regulates OSS-induced EC inflammation via the YAP signaling pathway. **(A)** Representative images showing dual-immunofluorescence staining of G3BP2 (green) and YAP (red) markers in the endothelial layer of *en face* carotids of the ligation model and statistical data of the YAP fluorescence intensities between the nucleus and cytoplasm ($n = 6$). Scale bars, 20 μm in the original image and 10 μm in the magnified image. Values are mean ± SEM and are analyzed using the unpaired two-tailed Student's *t*-test. ***$P < 0.001$. **(B)** Representative photomicrographs showing dual-immunofluorescence staining of G3BP2 (green) and YAP (red) in HUVECs and the ratio of the mean YAP fluorescence intensities between the nucleus and cytoplasm ($n = 6$). Scale bar, 20 μm in the original image and 10 μm in the magnified image. Values are mean ± SEM and are analyzed using the unpaired two-tailed Student's *t*-test. **$P < 0.01$. **(C)** Representative photomicrographs showing immunofluorescence staining of p-YAP and CD31 in carotid sections of ligation models and assessment of the percentage of the p-YAP-positive area in ECs ($n = 6$). Scale bars, 20 μm

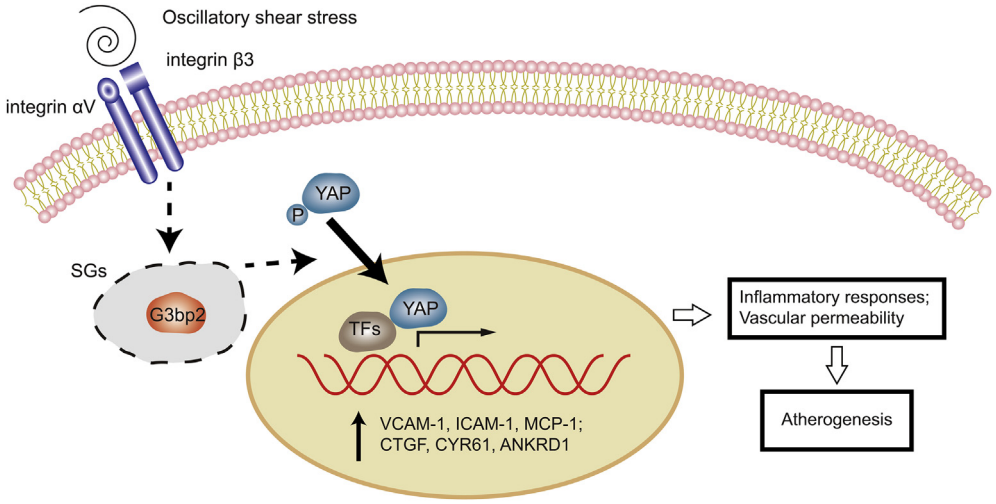

Figure 8 Scheme depicting of G3BP2-mediated YAP signaling in OSS-induced inflammatory ECs. Under ECs exposed to OSS, G3BP2 involves in the SGs formation and mediates the activation of integrin-YAP signal transduction pathway, which upregulates the expression of proinflammatory genes, and then promotes the inflammatory response and endothelium permeability changes, and eventually leads to atherogenesis.

profiles in OSS-treated sh-Control and sh-G3BP2 HUVECs. There were 1372 significantly expressed genes identified by RNA sequencing ($P < 0.05$ and fold change cut-off > 1.5), including 594 downregulated and 779 upregulated (Fig. S8). KEGG enrichment analysis revealed eight enriched pathways (Fig. 5A), including 'fluid shear stress and atherosclerosis', 'leukocyte transendothelial migration' and 'cell adhesion molecules (CAMs)'. Gene Ontology (GO) enrichment for biological process analysis indicated that G3BP2 is related to the regulation of cell—cell adhesion (Fig. 5B, S9, S10). Interestingly, heat map analysis of the mRNA profile showed that G3BP2 together with other components of SGs was significantly decreased in sh-G3BP2 HUVECs (Fig. 5C). Indeed, we observed that the THP-1 monocyte adhesion number was increased in sh-Control cells after treatment with OSS for 6 h but that monocyte adhesion was decreased in sh-G3BP2 cells (Fig. 5D, E). Further investigation demonstrated that the mRNA levels of proinflammatory cytokines, including ICAM-1, ICAM-1 and MCP-1, were decreased in sh-G3BP2 HUVECs compared with those in sh-Control HUVECs (Fig. 5F).

Previous studies have demonstrated that EC inflammation can lead to an increase in endothelial permeability[28] and that leukocyte transendothelial migration is associated with the permeability of the EC layer,[29,30] which will facilitate the infiltration of blood monocytes into the aortic intima.[31] Given the reduction in THP-1 monocyte adhesion of ECs with loss of G3BP2 in response to atheroprone shear stress *in vitro*, we assessed the permeability of ECs in the aorta of *G3bp2*$^{+/-}$*Apoe*$^{-/-}$ mice using Evans blue staining, and the results showed that loss of G3BP2 resulted in a decrease in Evans blue deposition in the aorta, particularly in the aortic arch and abdominal aorta (Fig. 6A, B).

Vascular endothelial VE-Cadherin is an indispensable adhesion molecule at endothelial junctions and plays a vital role in controlling endothelial permeability, leukocyte transendothelial migration and atherogenesis.[30] To accurately describe the differences in VE-Cadherin, five morphological categories were defined as previously described in the order of junctional strength from unstable to stable: fingers, straight junctions, thick junctions, thick to reticular junctions and reticular junctions (Fig. 6C).[32] In static HUVECs, the main VE-Cadherin pattern is a reticular junction in both sh-Control and sh-G3BP2 HUVECs. After being processed with OSS for 6 h, the ratio of the reticular junction to whole VE-Cadherin was decreased and the ratio

in the original image and 5 μm in the magnified image. Values are mean ± SEM and are analyzed using the unpaired two-tailed Student's *t*-test. $^{**}P < 0.01$. **(D)** Representative images showing immunofluorescence of p-YAP in sh-Control and sh-G3BP2 HUVECs treated with static or OSS and assessment of the percentage of the p-YAP positively stained area per field ($n = 6$). Scale bar, 20 μm. Values are mean ± SEM and are analyzed by one-way ANOVA followed by Bonferroni's multiple comparison test. $^{*}P < 0.05$; $^{***}P < 0.001$. **(E, F)** Western blotting quantification of G3BP2, YAP and p-YAP relative to GAPDH in different groups. Values are mean ± SEM and are analyzed by one-way ANOVA followed by Bonferroni's multiple comparison test. $^{***}P < 0.001$; *ns*, not significant. **(G)** Expression of the YAP target genes CTGF, CYR61 and ANKRD1 in sh-Control and sh-G3BP2 HUVECs treated with static or OSS ($n = 3$). Values are mean ± SEM and are analyzed by one-way ANOVA followed by Bonferroni's multiple comparison test. $^{*}P < 0.05$; $^{**}P < 0.01$; $^{***}P < 0.001$. **(H)** Representative images showing dual-immunofluorescence staining of G3BP2 (green) in sh-Control and sh-G3BP2 HUVECs treated with PBS or verteporfin and assessment of the percentage of the G3BP2 positively stained area per field ($n = 6$). Scale bar, 10 μm. Values are mean ± SEM and are analyzed by one-way ANOVA followed by Bonferroni's multiple comparison test. $^{*}P < 0.05$; $^{***}P < 0.001$. **(I)** Expression of the YAP target genes CTGF, CYR61, VCAM-1 and MCP-1 in sh-Control and sh-G3BP2 HUVECs treated with OSS and PBS/verteporfin ($n = 4$). Values are mean ± SEM and are analyzed by one-way ANOVA followed by Bonferroni's multiple comparison test. $^{***}P < 0.001$.

to fingers was increased in sh-Control, while the trend in sh-G3BP2 was the opposite (Fig. 6D, E). Moreover, *in vivo* studies showed that VE-Cadherin in ECs was significantly increased in the plaques of *G3bp2*$^{+/-}$*Apoe*$^{-/-}$ mice fed a high-fat diet for 8 weeks (Fig. S11).

Collectively, these observations suggested that G3BP2 deficiency may protect endothelial barrier function from OSS by stabilizing VE-Cadherin at endothelial junctions.

G3BP2 promotes EC permeability and inflammation under OSS via the YAP signaling pathway

Recent studies have found that the integrin β3-YAP cascade mediates the atheroprone effect of disturbed flow,[20] and YAP regulates the adherens junctional morphology of ECs.[32] Likewise, our RNA sequencing analysis also identified that integrin β3 of sh-G3BP2 was significantly reduced compared to that of sh-Control treated with OSS (Fig. S12A). Moreover, immunofluorescence experiments confirmed that deficiency of G3BP2 could reduce the expression of integrin β3 in the EC layer of plaques in *Apoe* $^{-/-}$ mice (Fig. S12B), and inhibition of integrin β3 could decrease the expression of G3BP2 (Fig. S12C). The result of Figure 6 showed the morphological changes in VE-cadherin in sh-G3BP2 cells. Therefore, we hypothesized that G3BP2 may mediate OSS-induced atherogenesis via the integrin β3-YAP cascade. Indeed, the immunofluorescence experiment showed that the nuclear transport of YAP was increased and the phosphorylation of YAP was decreased, and G3BP2 colocalized with YAP in the cytoplasm in ECs exposed to OSS (Fig. 7A—C). Interestingly, loss of G3BP2 alleviated the decrease in phosphorylated YAP and the increase in YAP induced by OSS (Fig. 7D). The Western blotting results showed that the ratio of p-YAP to total YAP was increased in sh-G3BP2 HUVECs, contrary to that in sh-Control HUVECs treated with OSS (Fig. 7E, F). And the RNA expression levels of well characterized YAP downstream genes, including CTGF, CYR61 and ANKRD1,[21] were significantly decreased in sh-G3BP2 HUVECs (Fig. 7G). In addition, YAP inhibitor verteporfin cannot decrease the expression level of G3BP2 induced by OSS (Fig. 7H), but can significantly reduce the mRNA expression level of YAP-targeting downstream genes, including CTGF, CYR61, VCAM-1 and MCP-1 (Fig. 7I). Together, these results suggested that G3BP2 may mediate endothelial inflammation induced by OSS by regulating downstream YAP phosphorylation (Fig. 8).

Discussion

Atherosclerotic plaques preferentially occur regions of curvature and bifurcation of vasculature with low and disturbed shear stress.[33] Haemodynamic stress induces physiological changes in ECs, with a major role in the initiation and formation of early-stage atherosclerosis. Environmental stress exposure leads to the formation of dynamic ribonucleoprotein aggregates called SGs. With many years of research in the area of cancer and virus infection, the potential function of SGs in cardiovascular disease was proposed in these two years ago, and our previous studies has revealed that downregulation of G3BP2 could inhibit atherosclerotic plaque formation.[34] In this study, we found that abnormal-expressed G3BP2 in the ECs are induced by OSS and the loss of G3BP2 could slow the progression of focal atherosclerotic lesion formation. Further investigation of the underlying mechanism suggested that the integrin β3-YAP pathway mediates this process.

To the best of our knowledge, this is the first report to demonstrate that G3BP2 is a shear stress sensitive gene and involves in OSS-induce endothelial dysfunction. This protein has been implicated in cardiovascular disease as one of the SG components.[7] Since our RNA sequencing data indicated that G3BP2 and other components of SG, were significantly increased in HUVECs treated with OSS, we hypothesized that G3BP2 might be involved in atherosclerotic plaque formation induced by OSS. Since a previous study have reported that G3BP1, another member of the G3BP family, contributes to the SMC stress response and atherosclerosis,[14] we detected the expression of G3BP1 and G3BP2 in the artery. Interestingly, we found that G3BP2 was highly and specifically expressed in ECs, while G3BP1 was highly and mainly expressed in SMCs, which is consistent with the previous study.

To further investigate the underlying mechanism of G3BP2 in atherogenesis, *G3bp2*$^{+/-}$*Apoe*$^{-/-}$ and *G3bp2*$^{-/-}$*Apoe*$^{-/-}$ mice were generated. Interestingly, our findings showed that atherosclerosis formation in ligated carotids in these mice can be significantly reduced compared with that in *Apoe*$^{-/-}$ mice without affecting lipid metabolism. Moreover, the lesions in descending aortas of *G3bp2*$^{+/-}$*Apoe*$^{-/-}$ and *G3bp2*$^{-/-}$*Apoe*$^{-/-}$ mice were reduced compared with those of *Apoe*$^{-/-}$ mice fed a normal diet for 35 weeks. Together, these data suggest that a G3BP2 deficiency can inhibit the focal distribution of atherosclerotic lesions induced by OSS.

The endothelial monolayers line the luminal surface of blood vessels constituting a permeable barrier.[35] Long-term shear stress stimulation promotes the dysfunction of the endothelial barrier. Endothelial barrier dysfunction could lead to vascular leakage, leukocyte transmigration and inflammation, finally resulting in cardiovascular disorders.[36—38] Our data showed that the expression level of inflammatory cytokines and the recruitment of macrophages in lesions were significantly relieved in *G3BP2*-knockdown or -knockout *Apoe*$^{-/-}$ mice. Further adhesion experiments showed that the number of monocyte adhesions was reduced in sh-G3BP2 HUVECs treated with OSS. Moreover, our findings showed that knockdown of G3BP2 did not affect the monocyte percentage in the blood and spleen. Therefore, we hypothesized that inhibition of atherosclerosis formation caused by G3BP2 might be linked to endothelial permeability. Both *in vivo* and *in vitro* results showed that loss of G3BP2 could reduce endothelial permeability. Adherens junctions play a crucial role in endothelial permeability and VE-Cadherin is the core component of adherens junctions.[32,39,40] VE-cadherin has been reported to correlate with the effect of shear stress on endothelial permeability.[41,42] The redistribution of VE-cadherin in response to short-time shear stress has a connection with the preferential localization of atherosclerosis in regions where blood flow patterns are low and disturbed.[43] And loss of VE-cadherin enhances endothelial permeability and leukocyte transendothelial migration,

which accelerates the formation of atherosclerotic plaques.[30] Our results showed that loss of G3BP2 could enhance adherens junctions under short-term exposure to OSS by altering the morphology of VE-Cadherin, and increase the expression of VE-Cadherin of ECs under long-term exposure to OSS. These data imply that loss of G3BP2 protects endothelial barrier function by stabilizing VE-Cadherin from OSS, further reducing the monocyte adhesion and infiltration into the vascular wall and contributing to its anti-atherosclerotic effect.

OSS could activate the integrin β3-YAP cascade and contribute to the expression of inflammatory genes.[20,21] Inhibition of integrin β3 or YAP activity and upregulation of p-YAP lead to an atheroprotective effect.[44] Our observations nicely correlated with the results of these previous studies. The G3BP2 downregulation effect induced by inhibition of integrin β3, and the colocalization of G3BP2 and YAP implies a potential correlation between G3BP2 and the integrin β3-YAP signaling pathway. Regulation of YAP-targeting downstream proinflammatory gene expression via regulating YAP nucleus translocation in sh-G3BP2 HUVECs further confirmed that the atheroprotective effect of G3BP2 inhibition was mediated by the integrin β3-YAP signaling pathway. Verteporfin could inhibit the transcriptional activity of YAP, but had no effect on G3BP2 expression level induced by OSS, which indicated that G3BP2 was the upstream regulator of YAP. Since loss of G3BP2 also reduced the expression level of integrin β3, there may be a positive regulation between integrin β3 and G3BP2, and further studies elucidating the exact mechanism underlying these results will be valuable.

Conclusion

Our study confirmed the role of G3BP2 in OSS induced atherogenesis, which regulates the endothelial barrier function and the secretion of pro-inflammatory cytokines via the YAP signaling pathway. Since G3BP2 has been found to be a new target for anticancer therapy[9] and has been identified as a novel and attractive therapeutic target for atherosclerosis in the present study, further studies using conditional knockout mice to investigate the underlying mechanism of G3BP2 and application of mechano-sensitivity for targeted drug delivery systems could be invaluable.[45,46]

Author contributions

All authors contributed to the design and implementation of this study. Tianhan Li: Methodology, Data curation, Writing Original draft preparation; Juhui Qiu: Conceptualization, Project administration, Funding acquisition.; Tingting Jia: Data curation, Formal analysis; Yinmin Liang: Resources, Visualization, Writing Reviewing and Editing; Kun Zhang: Validation, Data curation; Wenhua Yan: Investigation; Zhengjun Hou: Formal analysis; Shiwei Yang: Writing Reviewing and Editing; Liulu Shan; Writing Reviewing and Editing; Wenhao Xiong: Writing Reviewing and Editing; Yaokai Chen: Conceptualization, Visualization; Guixue Wang: Supervision, Funding acquisition.

Conflict of interests

The authors declare no conflicts of interest.

Funding

This work was supported by the National Natural Science Foundation of China (No. 31971242 and 12032007 to G.W.); The Natural Science Foundation of Chongqing, China (No. cstc2019jcyj-zdxmX0028 to G.W., cstc2019jcyj-xfkxX0004 to J.Q.); Open Fund of Tianjin Enterprise Key Laboratory on Hyaluronic Acid Application Research, China (No. KTRDHA-Y201903 to G.W.); The Fundamental Research Funds for the Central Universities, China (No. 2019CDYGZD008 to J.Q.); Chongqing Municipal Education Commission, China (No. KYYJ202001 to G.W.).

Acknowledgements

We thank the Laboratory of Genetic Regulators in the Immune System (Xinxiang Medical University) for providing technical support and assistance; We especially thank Ting-Ting Jia and Yin-Ming Liang for assistance with flow cytometry and genotyping of *G3bp2*/*Apoe* double-knockout mice.

Appendix A. Supplementary data

Supplementary data to this article can be found online at https://doi.org/10.1016/j.gendis.2021.11.003.

Abbreviations

ECA	external carotid artery
ECs	endothelial cells
G3BP2	ras-GAP/RNA binding protein
HDL	high density lipoprotein
HUVECs	human umbilical vein endothelial cells
ICA	internal carotid artery
ICAM-1	intercellular adhesion molecule-1
KEGG	Kyoto encyclopedia of gene and genomes
LCA	left carotid artery
LDL	low density lipoprotein
MCP-1	monocyte chemotactic protein 1
NF-κB	nuclear factor kappa B
OA	occipital artery
ORO	oil red O
OSS	oscillatory shear stress
RCA	right carotid artery
SGs	stress granules
SMCs	smooth muscle cells
STA	superior thyroid artery
TC	total cholesterol
TG	triglyceride
THP-1	human leukemic monocyte
TIA1	T-cell intracellular antigen 1
VCAM-1	vascular cell adhesion molecule-1
VP	verteporfin

References

1. Cherepanov D, Bentley TGK, Hsiao W, et al. Real-world cardiovascular disease burden in patients with atherosclerotic cardiovascular disease: a comprehensive systematic literature review. *Curr Med Res Opin*. 2018;34(3):459—473.
2. Wang Y, Zhang K, Qin X, et al. Biomimetic nanotherapies: red blood cell based core-shell structured nanocomplexes for atherosclerosis management. *Adv Sci*. 2019;6(12):1900172.
3. Gu HF, Tang CK, Yang YZ. Psychological stress, immune response, and atherosclerosis. *Atherosclerosis*. 2012;223(1): 69—77.
4. Peiffer V, Sherwin SJ, Weinberg PD. Does low and oscillatory wall shear stress correlate spatially with early atherosclerosis? A systematic review. *Cardiovasc Res*. 2013;99(2):242—250.
5. Tabas I. The role of endoplasmic reticulum stress in the progression of atherosclerosis. *Circ Res*. 2010;107(7):839—850.
6. Aldrich BT, Frakes EP, Kasuya J, Hammond DL, Kitamoto T. Changes in expression of sensory organ-specific microRNAs in rat dorsal root ganglia in association with mechanical hypersensitivity induced by spinal nerve ligation. *Neuroscience*. 2009;164(2):711—723.
7. Jain S, Wheeler JR, Walters RW, Agrawal A, Barsic A, Parker R. ATPase-modulated stress granules contain a diverse proteome and substructure. *Cell*. 2016;164(3):487—498.
8. Ash PE, Vanderweyde TE, Youmans KL, Apicco DJ, Wolozin B. Pathological stress granules in Alzheimer's disease. *Brain Res*. 2014;1584:52—58.
9. Gupta N, Badeaux M, Liu Y, et al. Stress granule-associated protein G3BP2 regulates breast tumor initiation. *Proc Natl Acad Sci U S A*. 2017;114(5):1033—1038.
10. Valentin-Vega YA, Wang YD, Parker M, et al. Cancer-associated DDX3X mutations drive stress granule assembly and impair global translation. *Sci Rep*. 2016;6:25996.
11. Cunningham KS, Gotlieb AI. The role of shear stress in the pathogenesis of atherosclerosis. *Lab Invest*. 2005;85(1):9—23.
12. Zhang K, Chen Y, Zhang T, et al. A novel role of Id1 in regulating oscillatory shear stress-mediated lipid uptake in endothelial cells. *Ann Biomed Eng*. 2018;46(6):849—863.
13. Hu S, Liu Y, You T, et al. Vascular semaphorin 7A upregulation by disturbed flow promotes atherosclerosis through endothelial β1 integrin. *Arterioscler Thromb Vasc Biol*. 2018;38(2): 335—343.
14. Herman AB, Silva Afonso M, Kelemen SE, et al. Regulation of stress granule formation by inflammation, vascular injury, and atherosclerosis. *Arterioscler Thromb Vasc Biol*. 2019;39(10): 2014—2027.
15. Irvine K, Stirling R, Hume D, Kennedy D. Rasputin, more promiscuous than ever: a review of G3BP. *Int J Dev Biol*. 2004; 48(10):1065—1077.
16. Guillén-Boixet J, Kopach A, Holehouse AS, et al. RNA-induced conformational switching and clustering of G3BP drive stress granule assembly by condensation. *Cell*. 2020;181(2):346—361.
17. Hahn RT, Hoppstädter J, Hirschfelder K, et al. Downregulation of the glucocorticoid-induced leucine zipper (GILZ) promotes vascular inflammation. *Atherosclerosis*. 2014;234(2):391—400.
18. Herman AB, Autieri MV. Inflammation-regulated mRNA stability and the progression of vascular inflammatory diseases. *Clin Sci (Lond)*. 2017;131(22):2687—2699.
19. Sokabe T, Yamamoto K, Ohura N, et al. Differential regulation of urokinase-type plasminogen activator expression by fluid shear stress in human coronary artery endothelial cells. *Am J Physiol Heart Circ Physiol*. 2004;287(5):H2027—H2034.
20. Wang L, Luo JY, Li B, et al. Integrin-YAP/TAZ-JNK cascade mediates atheroprotective effect of unidirectional shear flow. *Nature*. 2016;540(7634):579—582.
21. Wang KC, Yeh YT, Nguyen P, et al. Flow-dependent YAP/TAZ activities regulate endothelial phenotypes and atherosclerosis. *Proc Natl Acad Sci U S A*. 2016;113(41):11525—11530.
22. Zhou J, Lee PL, Tsai CS, et al. Force-specific activation of Smad 1/5 regulates vascular endothelial cell cycle progression in response to disturbed flow. *Proc Natl Acad Sci U S A*. 2012; 109(20):7770—7775.
23. Sucosky P, Balachandran K, Elhammali A, Jo H, Yoganathan AP. Altered shear stress stimulates upregulation of endothelial VCAM-1 and ICAM-1 in a BMP-4- and TGF-beta1-dependent pathway. *Arterioscler Thromb Vasc Biol*. 2009;29(2):254—260.
24. Walpola PL, Gotlieb AI, Cybulsky MI, Langille BL. Expression of ICAM-1 and VCAM-1 and monocyte adherence in arteries exposed to altered shear stress. *Arterioscler Thromb Vasc Biol*. 1995;15(1):2—10.
25. Nam D, Ni CW, Rezvan A, et al. Partial carotid ligation is a model of acutely induced disturbed flow, leading to rapid endothelial dysfunction and atherosclerosis. *Am J Physiol Heart Circ Physiol*. 2009;297(4):H1535—H1543.
26. Zhang SH, Reddick RL, Piedrahita JA, Maeda N. Spontaneous hypercholesterolemia and arterial lesions in mice lacking apolipoprotein E. *Science*. 1992;258(5081):468—471.
27. Wei D, Wang G, Tang C, et al. Upregulation of SDF-1 is associated with atherosclerosis lesions induced by LDL concentration polarization. *Ann Biomed Eng*. 2012;40(5):1018—1027.
28. Mundi S, Massaro M, Scoditti E, et al. Endothelial permeability, LDL deposition, and cardiovascular risk factors-a review. *Cardiovasc Res*. 2018;114(1):35—52.
29. Huveneers S, Daemen MJ, Hordijk PL. Between Rho(k) and a hard place: the relation between vessel wall stiffness, endothelial contractility, and cardiovascular disease. *Circ Res*. 2015;116(5):895—908.
30. Schulz B, Pruessmeyer J, Maretzky T, et al. ADAM10 regulates endothelial permeability and T-Cell transmigration by proteolysis of vascular endothelial cadherin. *Circ Res*. 2008;102(10): 1192—1201.
31. Rao RM, Yang L, Garcia-Cardena G, Luscinskas FW. Endothelial-dependent mechanisms of leukocyte recruitment to the vascular wall. *Circ Res*. 2007;101(3):234—247.
32. Neto F, Klaus-Bergmann A, Ong YT, et al. YAP and TAZ regulate adherens junction dynamics and endothelial cell distribution during vascular development. *Elife*. 2018;7:e31037.
33. Cecchi E, Giglioli C, Valente S, et al. Role of hemodynamic shear stress in cardiovascular disease. *Atherosclerosis*. 2011; 214(2):249—256.
34. Li T, Safitri M, Zhang K, et al. Downregulation of $G3BP_2$ reduces atherosclerotic lesions in $ApoE^{-/-}$ mice. *Atherosclerosis*. 2020; 310:64—74.
35. Pulous FE, Grimsley-Myers CM, Kansal S, Kowalczyk AP, Petrich BG. Talin-dependent integrin activation regulates VE-cadherin localization and endothelial cell barrier function. *Circ Res*. 2019;124(6):891—903.
36. Komarova YA, Kruse K, Mehta D, Malik AB. Protein interactions at endothelial junctions and signaling mechanisms regulating endothelial permeability. *Circ Res*. 2017;120(1):179—206.
37. Shechter R, London A, Schwartz M. Orchestrated leukocyte recruitment to immune-privileged sites: absolute barriers versus educational gates. *Nat Rev Immunol*. 2013;13(3): 206—218.
38. Harrison DG. Endothelial dysfunction in atherosclerosis. *Basic Res Cardiol*. 1994;89(Suppl 1):87—102.
39. Dejana E. Endothelial adherens junctions: implications in the control of vascular permeability and angiogenesis. *J Clin Invest*. 1997;100(11 Suppl):S7—S10.
40. Lakshmikanthan S, Sobczak M, Li Calzi S, Shaw L, Grant MB, Chrzanowska-Wodnicka M. Rap1B promotes VEGF-induced

endothelial permeability and is required for dynamic regulation of the endothelial barrier. *J Cell Sci*. 2018;131(1):jcs207605.
41. Ogunrinade O, Kameya GT, Truskey GA. Effect of fluid shear stress on the permeability of the arterial endothelium. *Ann Biomed Eng*. 2002;30(4):430—446.
42. Kiessling F, Becker D, Ullisch EV, Kübler W, Haller C. Influence of intercellular junctions on endothelin secretion of human umbilical vein endothelial cells in vitro. *Basic Res Cardiol*. 2000;95(4):299—307.
43. Miao H, Hu YL, Shiu YT, et al. Effects of flow patterns on the localization and expression of VE-cadherin at vascular endothelial cell junctions: in vivo and in vitro investigations. *J Vasc Res*. 2005;42(1):77—89.
44. Liu D, Lv H, Liu Q, et al. Atheroprotective effects of methotrexate via the inhibition of YAP/TAZ under disturbed flow. *J Transl Med*. 2019;17(1):378.
45. Saxer T, Zumbuehl A, Müller B. The use of shear stress for targeted drug delivery. *Cardiovasc Res*. 2013;99(2):328—333.
46. Nurhidayah D, Maruf A, Zhang X, Liao X, Wu W, Wang G. Advanced drug-delivery systems: mechanoresponsive nanoplatforms applicable in atherosclerosis management. *Nanomedicine*. 2019;14(23):3105—3122.